Electron spin resonance of Ni-doped $CuGeO_3$ in the paramagnetic, spin-Peierls, and antiferromagnetic states: Comparison with nonmagnetic impurities

B. Grenier
Département de Recherche Fondamentale sur la Matière Condensée, SPSMS-MDN, CEA/Grenoble, 17 rue des Martyrs, 38054 Grenoble, France
and Université Joseph Fourier Grenoble I, France

P. Monod
Laboratoire de Physique du Solide, Ecole Supérieure de Physique et Chimie, 10 rue Vauquelin, 75231 Paris, France

M. Hagiwara, M. Matsuda,* and K. Katsumata†
RIKEN (The Institute of Physical and Chemical Research), Wako, Saitama 351-0198, Japan

S. Clément and J.-P. Renard
Institut d'Electronique Fondamentale, Bât. 220, Université Paris-Sud, 91405 Orsay, France

A. L. Barra
Laboratoire des Champs Magnétiques Intenses, CNRS/MPI, 25 rue des Martyrs, 38042 Grenoble, France

G. Dhalenne and A. Revcolevschi
Laboratoire de Physico-Chimie de l'Etat Solide, Bât. 414, Université Paris-Sud, 91405 Orsay, France
(Received 9 April 2001; published 15 February 2002)

We have performed electron-spin-resonance measurements on single crystals of the doped spin-Peierls compounds $CuGe_{1-y}Si_yO_3$ and $Cu_{1-x}M_xGeO_3$ with $M=$Zn, Mg, Ni ($x,y\leqslant 0.1$). The first part of our experiments was performed in the paramagnetic and spin-Peierls phases at 9.5, 95, and 190 GHz. All nonmagnetic impurities (Si, Zn and Mg) were found to hardly affect the position and linewidth of the single line resonance, in spite of the moment formation due to the broken chains. In contrast to Si, Zn, and Mg dopings, the presence of Ni ($S=1$) at low concentration induces a spectacular shift toward high fields of the ESR line (up to 40% for $x=0.002$), together with a large broadening. This shift is strictly proportional to the ratio of Ni to Cu susceptibilities: Hence it is strongly enhanced below the spin-Peierls transition. We interpret this shift and the broadening as due to the exchange field induced by the Ni ions onto strongly exchange coupled Cu spins. Second, the antiferromagnetic resonance was investigated in Ni-doped samples. The frequency vs magnetic-field relation of the resonance is well explained by the classical theory with orthorhombic anisotropy, with g values remarkably reduced, in accordance with the study of the spin-Peierls and paramagnetic phases. The easy, second-easy, and hard axes are found to be a, c, and b axes, respectively. These results, which are dominated by the single ion anisotropy of Ni^{2+}, are discussed in comparison with those in the Zn- and Si-doped $CuGeO_3$.

DOI: 10.1103/PhysRevB.65.094425 PACS number(s): 75.10.Jm, 76.30.Da

I. INTRODUCTION

The quasi-one dimensional compound $CuGeO_3$ is the first inorganic system to exhibit a spin-Peierls (SP) transition.[1] It is extensively studied since large single crystals are readily available, which allows one to perform various kinds of experiments. The magnetic structure of $CuGeO_3$ is as follows: the spin correlations are antiferromagnetic along the b and c axes, and ferromagnetic along the a axis. Below $T_{SP}\simeq 14.3$ K, $S=\frac{1}{2}$ Heisenberg antiferromagnetic (AF) chains, running along the c axis, become dimerized and an energy gap of $\Delta=2$ meV opens between the singlet ground state and the first excited triplet states. The SP transition is evidenced by a kink at T_{SP} in the magnetic susceptibility, and is clearly revealed by x-ray and neutron scattering.[2] A unique feature of this compound is that the effect of impurities can be studied by substituting impurity ions (Zn, Mg, and Ni) for the Cu sites[3–8] and a Si ion for the Ge sites.[9] These substitutions all induce a strong decrease of T_{SP} and the appearance, at lower temperature ($T<T_N<T_{SP}$), of a three-dimensional AF phase. The most intriguing feature in the impurity effects is the coexistence below T_N of a SP state and long-range AF ordering, which was extensively studied both experimentally[10,11] and theoretically.[12] Magnetization measurements performed in $Cu_{1-x}M_xGeO_3$ (with $M=$Zn, Mg, Ni) and $CuGe_{1-y}Si_yO_3$ single crystals revealed the existence of a universal temperature-doping concentration phase diagram with a scaling factor $x=3y$.[13] The spin-Peierls temperature shows a linear decrease as the doping level increases, following the relation $T_{SP}(x,y)/T_{SP}(0)=1-15x=1-44y$, while the Néel temperature increases linearly from 0 at low doping levels up to a broad maximum around 4.5 K for $x=3y\simeq 0.04$ and then gradually decreases. Thus doping on the Ge site by Si impurities (spin 0) is three

times more efficient than doping on the Cu site, either by magnetic (Ni: spin 1) or nonmagnetic (Zn, Mg) impurities. For all nonmagnetic impurities, the easy axis in the AF phase is the *c* axis.[6,9,10,13–17] However, some deviations from this universal behavior are noted in the case of Ni concerning the AF phase. Indeed, the $T_N(x)$ curve for Ni is slightly lower,[13] and the easy axis was found to be the *a* axis from susceptibility[13,18] and neutron-scattering experiments.[7]

Electron-spin-resonance (ESR) studies of paramagnetic and spin-Peierls phases were performed by different authors in pure,[19–22] Si-doped, and Zn-doped $CuGeO_3$,[16,23,24] and the antiferromagnetic resonance was also studied for these two substitutions.[15–17] But very little has been done using the ESR technique in Ni-doped $CuGeO_3$ besides the work of Glazkov *et al.*,[25] where a large number of parameters was needed for the interpretation.

The first aim of this paper is to make a comparative ESR study of $Cu_{1-x}M_xGeO_3$ (with M=Zn, Mg, Ni) and $CuGe_{1-y}Si_yO_3$ compounds, to find out if the universal character of the temperature-concentration phase diagram holds also for ESR, especially when comparing nonmagnetic and magnetic impurities. Extensive ESR measurements were performed in the paramagnetic and spin-Peierls phases on high-quality single crystals, at various doping levels. The results obtained in the nonmagnetic impurity doped compounds are briefly presented, and those obtained in Ni-doped $CuGeO_3$ are focused on. For the latter, our results on the ESR line shift are analyzed in detail, and a model is proposed to explain the observed effect.

The second aim of this paper is to study the antiferromagnetic resonance (AFMR) in Ni-doped $CuGeO_3$ samples, and to compare the results with those obtained in the case of nonmagnetic impurities. ESR is indeed a crucial technique to study magnetic anisotropy at a microscopic level. In both studies (ESR and AFMR), Ni substitution is shown to produce different effects on the spin resonance of $CuGeO_3$, as compared to the case of nonmagnetic impurities.

II. EXPERIMENTAL SETUP

The $CuGe_{1-y}Si_yO_3$ (y=0, 0.002, 0.007, 0.0085, 0.015, 0.06, and 0.085) and $Cu_{1-x}M_xGeO_3$ (M=Zn with x=0.016, 0.039, and 0.01; M=Mg with x=0.01, 0.03, and 0.05; and M=Ni with x=0.002, 0.0085, 0.02, 0.03, and 0.04) single crystals used in this study were grown from a melt under an oxygen atmosphere using a floating-zone method associated with an image furnace. All samples were then analyzed using inductively coupled plasma atomic emission spectroscopy (ICP/AES). The doping levels that are reported here are thus the effective ones derived from the ICP/AES analysis, which are usually slightly lower than the nominal concentration.

The ESR measurements were performed between 4 and 300 K in all single crystals on a standard *X*-band spectrometer (Bruker ESP 300E), operating at a frequency $f \simeq 9.5$ GHz and in a field range ± 1.6 T. With this apparatus, the measured signal is the field derivative of the absorption. The crystal of typical mass 5–10 mg can be mounted onto the sample holder, in order that the magnetic field lies either in the (a,b) or (a,c) plane. Because of the huge broadening of the ESR line induced by Ni doping, further measurements were performed on a homemade high-field spectrometer. These experiments were crucial to interpreting the observed phenomena. The measurements were performed between 4 and 250 K at frequencies of 95 and 190 GHz, with the field parallel to the *c* axis. The sample size was about $4 \times 8 \times 8$ mm^3, corresponding to a mass of more than 500 mg. With this spectrometer, the measured ESR signal is a field derivative of a combination of the dispersion and the absorption. The AFMR measurements were performed on two $Cu_{1-x}Ni_xGeO_3$ single crystals, with x=0.03 and 0.04, in frequency ranges of 9, 20, 35, and 50 GHz and a temperature of 1.8 K (i.e., below T_N). The dimension of the crystals used in these experiments is about $3 \times 3 \times 2$ mm^3. We used an *X*-band spectrometer (JOEL-JES-RE3X) for the experiments performed at 9 GHz, and a homemade spectrometer for higher frequencies. For the latter, microwaves are generated from two klystrons at 20 and 50 GHz, and from a Gunn oscillator at 35 GHz, the magnetic field (B) being produced by a 20 T superconducting magnet from Oxford Instruments. The magnetic susceptibility measurements in the Ni-doped samples are also presented in this paper (for the other compounds, see Ref. 13): they were performed on a homemade superconducting quantum interference device (SQUID) magnetometer operating in a temperature range 1.8–300 K and in a magnetic-field range of 0–8 T.

III. ESR IN $CuGeO_3$ DOPED WITH NONMAGNETIC IMPURITIES

The temperature dependence of the magnetic susceptibility was first measured in all samples whose ESR study is presented here (see Ref. 26 for the Si doping, and Ref. 13 for the Si, Zn, and Mg doping). In this section we briefly present the ESR results obtained in the case of nonmagnetic impurities, and discuss the linewidth, the shift, and the integrated intensity of the resonance line.

A wide series of $CuGeO_3$ samples doped with nonmagnetic impurities Si, Zn, and Mg (see the list in Sec. II), and a sample of pure $CuGeO_3$, were investigated. In all Si-, Zn- and Mg-doped $CuGeO_3$ compounds, a single Lorentzian derivative ESR line was observed at the *X* band between 5 and 300 K along the three crystallographic axes, as for pure $CuGeO_3$. Figure 1 shows examples of spectra obtained in a 1.6% Zn-doped sample for $B \| b$, i.e., for a field perpendicular to the chain axis, and at different temperatures, above and below T_{SP}=10.4 K. In all these samples and along the three crystallographic directions, the linewidth ΔB and its temperature dependence were found to be identical to those of pure $CuGeO_3$ above 15 K,[27] but not below: $\Delta B(T)$ depends on the Néel and SP temperatures, which vary with the doping level. As can be seen in Fig. 1, a 1% shift of the ESR line is observed only below T_{SP}. The same result was found in all $CuGeO_3$ samples doped with nonmagnetic impurities, and also in the pure compound: The g values remain constant down to 10–15 K, and become shifted at lower temperature by less than 2%. The sign of the shift depends on the field orientation and on the substituent, which agrees well with the results of Hase *et al.*[23] obtained for pure, Zn-doped and Si-

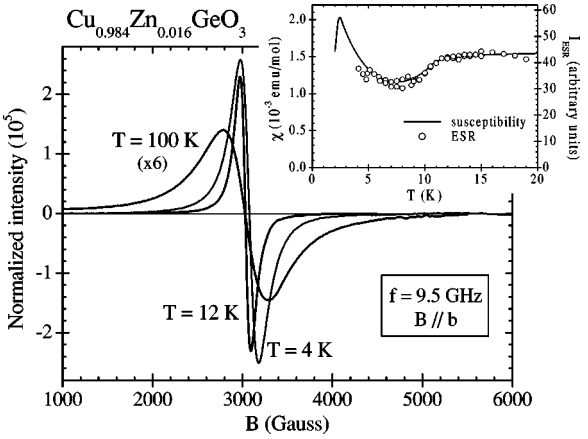

FIG. 1. ESR spectra obtained at the X band, with $B \| b$, in $Cu_{0.984}Zn_{0.016}GeO_3$, above and below the SP temperature. The inset illustrates the temperature dependence of the (twice) integrated ESR intensity as compared to that of the static susceptibility.

doped $CuGeO_3$. For pure and Si-doped $CuGeO_3$, the g factor is found to increase along b and to decrease along a and c, as the temperature decreases. For Zn- and Mg-doped $CuGeO_3$ the opposite behavior is observed for the three crystallographic directions.

The inset of Fig. 1 shows the variation with temperature of the ESR (twice) integrated intensity I_{ESR} as compared to that of the static susceptibility, in the 1.6% Zn-doped $CuGeO_3$ sample. Since both curves can be superimposed, we infer that ESR at the X band cannot distinguish between triplet spins (the spin-Peierls contribution) and spins freed by impurities (the Curie-Weiss contribution).[13,26] We will come back to this point in Sec. V B. A similar investigation carried out by Hassan *et al.*[24] on Zn-doped $CuGeO_3$ (up to 5% Zn) on powder samples at high field (between 100 and 400 GHz) yielded results qualitatively different from the previous investigations at lower frequency (see Refs. 15 and 16 and the present work). In Ref. 24, the appearance of two distinct powder pattern ESR spectra was interpreted as a separate contribution from excited spin-Peierls triplet and Zn-induced moments. Motivated by this apparent paradox, we investigated the ESR in the paramagnetic phase of a single crystal of $CuGeO_3$: 5% Zn at 95 GHz and 5 K. Contrary to Ref. 24, for all field directions in the (a,b) plane we observe a single resonance line varying from $g_a = 2.145$ to $g_b = 2.240$, in accordance with our X-band measurements. Thus we are forced to conclude that the additional ESR powder pattern observed by Hassan *et al.*[24] is somehow linked to the powdered nature of the investigated samples.

IV. MAGNETIC SUSCEPTIBILITY IN Ni-DOPED $CuGeO_3$

Figure 2 shows the temperature dependence of the magnetic susceptibility measured in pure $CuGeO_3$ and in $Cu_{1-x}Ni_xGeO_3$ samples in the 1.8–300 K temperature range [Fig. 2(b)] and below 30 K [Fig. 2(a)]. The data from Fig. 2(a) clearly show a decrease of the SP transition (which is visible up to $x = 0.03$) and the occurrence of an AF transition at lower temperature, with a being the easy axis. Indeed, the

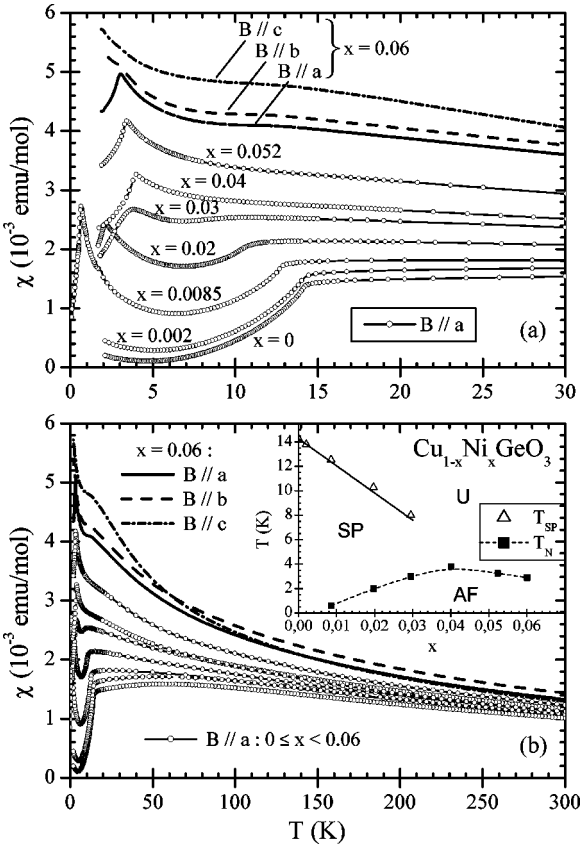

FIG. 2. Temperature dependence of the magnetic susceptibility measured in $Cu_{1-x}Ni_xGeO_3$ samples in a 1 kG field applied along the a axis (easy axis) for $0 \leqslant x \leqslant 0.052$ and along the three crystallographic axes for $x = 0.06$. The inset of (b) displays the (T,x) phase diagram obtained from these measurements.

susceptibility measured with the external field along the a axis shows a peak around 3 K for $x = 0.06$ (see the solid line), while the susceptibilities measured with the external field along the b and c axes further increase below 3 K with decreasing temperature (see the dashed and dash-dotted lines). The Ni^{2+} ion, with $S = 1$, is considered to participate to the long-range magnetic ordering, since the magnitude of the Curie tail is one order of magnitude smaller than expected from 6% Ni free spins, indicating that the interaction between the Cu^{2+} and Ni^{2+} ions is relatively large. The (T,x) phase diagram shown in the inset of Fig. 2(b) was obtained from these measurements. The values of the spin-Peierls and Néel temperatures (when they exist) are given in Table I. For $x = 0.002$, the susceptibility measurement was performed only down to $T = 1.8$ K, so that the Néel temperature (expected to be smaller than the 0.6 K value obtained for $x = 0.0085$) could not be determined.

Figure 2(b) illustrates the large effect of Ni doping on the global susceptibility curve, due to the magnetic nature of the Ni^{2+} ion. Indeed, the susceptibility increases more and more between 300 and 20 K as the Ni concentration increases. Interestingly, the susceptibilities along the a and b axes become smaller than the one along c below $\simeq 50$ K. This anomalous temperature dependence was not observed in Si- and Zn-doped $CuGeO_3$.[9,13,28] This could originate from the

TABLE I. Spin-Peierls and Néel temperatures (when they exist) for pure and Ni-doped $CuGeO_3$ samples.

x	T_{SP} (K)	T_N (K)
0	14.25	–
0.002	13.8	<1.8
0.0085	12.55	0.6
0.02	10.3	2
0.03	8	3
0.04	–	3.8
0.052	–	3.25
0.06	–	2.9

single ion anisotropy of Ni^{2+} ions DS_z^2, with z along the direction of the distorted oxygen octahedron in the (a,b) plane, as clearly observed with Mn^{2+} (Ref. 29). This will be further discussed in the AFMR results presented in Sec. VI.

The temperature dependence of the susceptibility could be analyzed in the paramagnetic phase ($T>20$ K) by a crude model of Cu-Ni pairs, neglecting in a first step the single-ion anisotropy of Ni^{2+}, yielding an estimate of the Ni-Cu antiferromagnetic exchange coupling of 25 K.[13] This value is to be compared to the strongest Cu-Cu coupling, $J_c = 120–180$ K along the c axis. The susceptibility data from Fig. 2 will be used later to explain the ESR results.

V. ESR IN Ni-DOPED $CuGeO_3$

A. Experimental results

The Ni-doped $CuGeO_3$ samples were investigated at the X band along the three crystallographic directions and at high frequency along the c axis. Figure 3 shows typical ESR spectra obtained in $Cu_{0.998}Ni_{0.002}GeO_3$ ($T_{SP}=13.8$ K) at the X band along the c axis at $T=100$, 12, and 4 K. Figure 4 shows ESR spectra obtained in $Cu_{0.9915}Ni_{0.0085}GeO_3$ ($T_{SP}=12.55$ K) at 95 GHz along the c axis at $T=100$, 11, and 7 K. In all Ni-doped compounds, a single Lorentzian derivative ESR line was again observed, but now, both the linewidth ΔB and the resonance field B_{res} behave in a completely different way. Qualitatively, as compared to Fig. 1 for 1.6% Zn doping, one immediately notes in Fig. 3 for 0.2% Ni doping (the X band) and Fig. 4 for 0.85% (95 GHz), that a $\sim 5\%$ shift toward high field is already visible in the spectra at 12 and 11 K respectively, compared to those at 100 K. This shift increases to reach 24% at 7 K (Fig. 4) and 36% at 4 K (Fig. 3) which is much larger than the $\sim 1\%$ shift measured in Fig. 1. Moreover, one notes the large broadening induced by Ni doping: the spectrum measured at 100 K for 0.2% Ni doping (see Fig. 3) is about three times broader than for 1.6% Zn doping (see Fig. 1) or pure $CuGeO_3$. This large broadening justifies the use of higher frequencies for further studies of the Ni-doped $CuGeO_3$ samples.

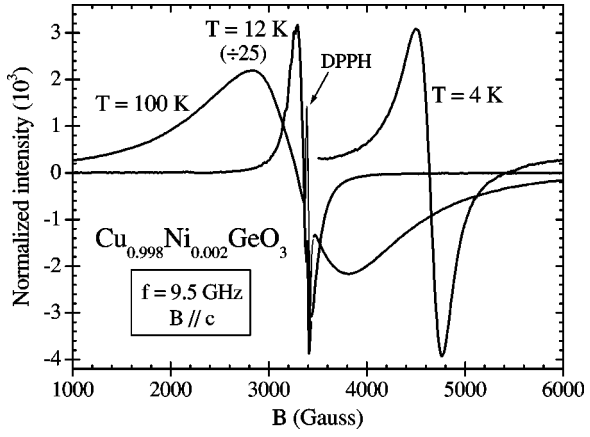

FIG. 3. ESR spectra obtained in the X band, with $B\|c$, in $Cu_{0.998}Ni_{0.002}GeO_3$, above and below the SP temperature. The figure shows the huge broadening of the ESR line on each side of T_{SP} and the increasing shift towards high fields as T decreases.

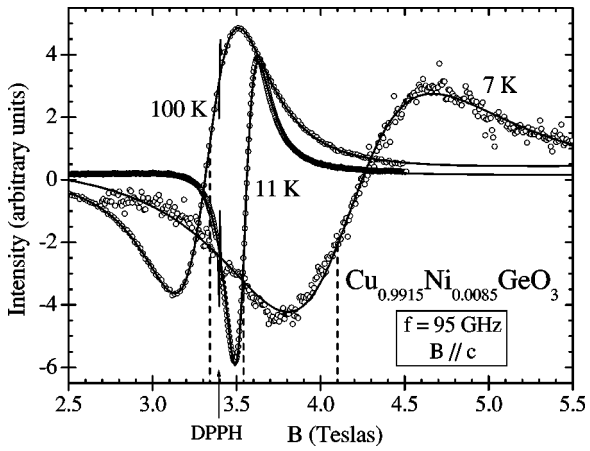

FIG. 4. ESR spectra obtained at 95 GHz, with $B\|c$, in $Cu_{0.9915}Ni_{0.0085}GeO_3$, above and below the SP temperature. Note the large broadening on each side of T_{SP} and the increasing shift toward high fields as T decreases. The solid lines are the best Lorentzian fits to the experimental data [see Eq. (1)], and the dashed lines point out the position of the resonance field at each temperature, obtained from the fit.

The spectra obtained in the X band ($f=9.5$ GHz) correspond to the field derivative of the absorption χ'', while those obtained in the millimetric domain ($f=95$ and 190 GHz) correspond to the field derivative of a combination of the absorption χ'' and dispersion χ'. In order to check the Lorentzian profile and to extract precisely the integrated intensity (meaningful at the X band only), the linewidth, and the resonance field for each measured spectrum, the data obtained in the X and millimetric domains were fitted to the relation

$$S(B)=S_0(B)+\frac{d\chi''}{dB}\cos\alpha+\frac{d\chi'}{dB}\sin\alpha, \qquad (1)$$

where $S_0(B)$ is a linear function in B accounting for the base line, α is the phase (equal to zero at the X band), and $\chi''(B)$ and $\chi'(B)$ are Lorentzian shapes centered at the resonance field B_{res}, with an integrated intensity I_{ESR} and a Lorentzian linewidth $\Delta B^{Lorentz}$. The "peak to peak" linewidth ΔB of the ESR spectra is given by $\Delta B=(\sqrt{3}/2)\Delta B^{Lorentz}$. Figure 4 illustrates the very good quality of the fits to Eq. (1) of a few

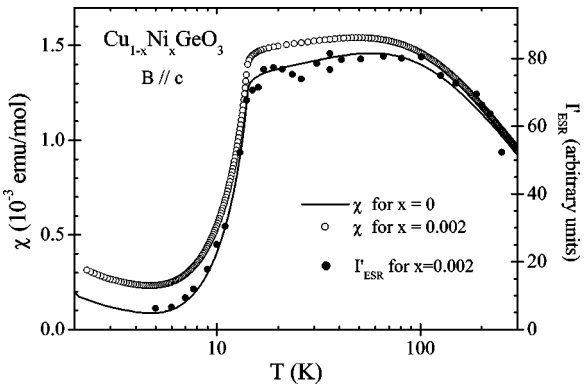

FIG. 5. Temperature dependence of the static susceptibility (SQUID) measured with $B=0.1$ T$\|c$ in pure and 0.2% Ni-doped $CuGeO_3$ (left scale) compared to the susceptibility derived from the ESR measurements ($I'_{ESR}=I_{ESR}B_0/B_{res}$) in the same Ni-doped sample and with $B\|c$ (right scale), on a logarithmic T scale. $I'_{ESR}(T)$ fits better with the static susceptibility of pure $CuGeO_3$.

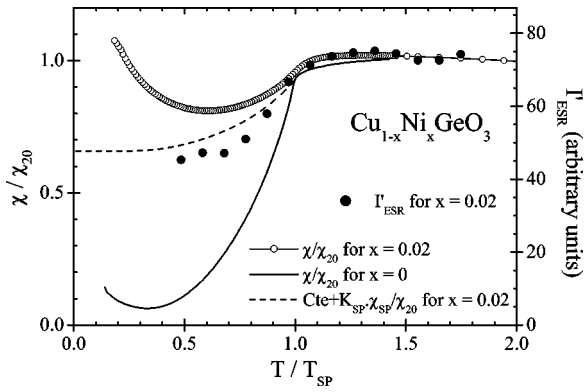

FIG. 6. Static susceptibility (SQUID) measured with $B=0.1$ T$\|c$ in pure ($T_{SP}=14.25$ K) and 2% Ni-doped $CuGeO_3$ ($T_{SP}=10.3$ K), normalized at 20 K (left scale), compared to the susceptibility derived from the ESR measurements (I'_{ESR}) in the same Ni-doped sample and with $B\|c$ (right scale), as a function of the reduced temperature T/T_{SP}. The dashed line (left scale) represents the SP contribution to the global susceptibility of 2% Ni-doped $CuGeO_3$ arising from the model described in Ref. 13 (see the text).

ESR spectra measured in $Cu_{0.9915}Ni_{0.0085}GeO_3$ at 95 GHz for three different temperatures. The typical precision is less than 1% on the determination of ΔB and less than 0.01% for B_{res}, the precision on the phase α (in the case of the millimetric range) always being better than 1°.

1. Integrated intensity at the X band

In the case of the *X* band, the ESR integrated intensity can be compared to the static susceptibility measured with the SQUID magnetometer. ESR spectra were measured in three $Cu_{1-x}Ni_xGeO_3$ samples. For $x=0.002$, the ESR line could be followed between 4 and 300 K, but due to the very large broadening induced by Ni doping, the ESR line could be followed only up to 30 K for $x=0.0085$ and up to 20 K for $x=0.02$. All spectra measured for $x=0.002$ were analyzed using Eq. (1) with $\alpha=0$ and $S_0(B)=0$ and the ESR (twice) integrated intensity I_{ESR} was obtained for each temperature. Due to the strong line shift induced by Ni doping, the resonance field must be taken into account and the static susceptibility measured by SQUID thus has to be compared with the ratio

$$I'_{ESR}=I_{ESR}\left(\frac{B_0}{B_{res}}\right), \tag{2}$$

where B_0 is the resonance field of pure $CuGeO_3$ measured at the same frequency and along the same direction (i.e., corresponding to $g_c=2.05$ in the present case where $B\|c$). Note that in the case of nonmagnetic impurities, the static susceptibility was directly compared to I_{ESR} since the resonance field varied by less than 2% on the whole temperature range.

Figure 5 displays the temperature dependence of I'_{ESR} (right scale) compared to the macroscopic susceptibility vs temperature $\chi(T)$ in the same sample ($x=0.002$) and in pure $CuGeO_3$ (left scale), on a logarithmic scale. The SQUID measurements were performed in a 0.1 T magnetic field applied along the *c* axis, while the ESR measurements were performed in a sweeping field from 0 to 6600 G applied along the same axis. By adjusting the $\chi(T)$ and $I'_{ESR}(T)$ curves at high temperature, one can note that the ESR integrated intensity better follows the susceptibility of the pure sample than that of the 0.2% Ni-doped sample. This results leads one to suggest that the ESR signal would originate only from the Cu^{2+} spins of $CuGeO_3$ while the Ni^{2+} spins would not participate in this resonance line.[30]

To check this assumption, the same comparison was performed for a higher Ni-doped sample ($x=0.02$). Here again, the static susceptibility vs temperature curves of $Cu_{0.98}Ni_{0.02}GeO_3$ and pure $CuGeO_3$ are compared with the $I'_{ESR}(T)$ curve derived from ESR measurements in the same Ni-doped sample. For an easier comparison, the susceptibility data were normalized at 20 K [by dividing for each temperature $\chi(T)$ by $\chi(T=20\ \text{K})=\chi_{20}$] and all the curves are plotted as a function of the reduced temperature T/T_{SP}, with $T_{SP}=14.25$ K for $x=0$ and $T_{SP}=10.3$ K for $x=0.02$ (see Fig. 6). Indeed, for such a high Ni-doping level, the spin-Peierls temperature and the absolute value of the static susceptibility are quite different from the pure sample [see Fig. 2(a)]. By normalizing the susceptibility and ESR data at 20 K, one can note that the I'_{ESR} curve lies in between the normalized susceptibilities of pure and Ni-doped $CuGeO_3$.

Since it was shown[13,26] that the amplitude of the SP order parameter (expressed by the fraction K_{SP}) is reduced in the presence of doping (by Ni, Zn, Mg, and Si), we have analyzed our data accordingly. In particular, for $Cu_{1-x}Ni_xGeO_3$ with $x=0.02$, K_{SP} was found to be equal to 0.465,[13] i.e., only approximately one-half of the Cu spins are able to dimerize so that the decrease of $\chi(T)$ is much smaller than for pure $CuGeO_3$. Moreover, the decrease of the energy gap upon doping further amplifies this effect. Thus our ESR intensity data have to be compared with this (reduced) SP contribution instead of that of the full susceptibility of pure $CuGeO_3$. The dashed line in Fig. 6 shows the temperature dependence of this SP contribution (divided by the $Cu_{0.98}Ni_{0.02}GeO_3$ susceptibility at 20 K) normalized at

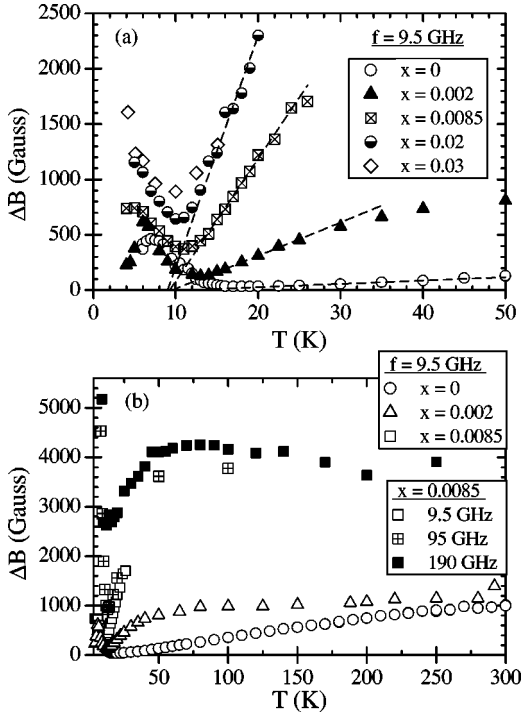

FIG. 7. Temperature dependence of the ESR linewidth measured with $B\|c$ in pure and Ni-doped $CuGeO_3$ for various concentrations: (a) Low-temperature part at the *X* band. (b) High-temperature part at the *X* band and higher frequencies. Note the plateau above 50 K for 0.2 and 0.85% Ni.

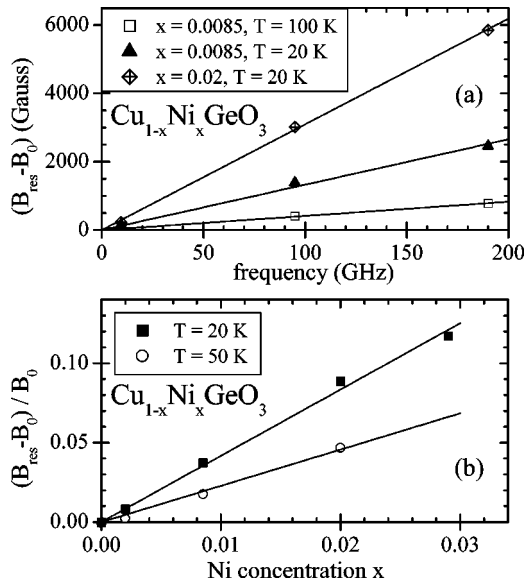

FIG. 8. (a) Frequency dependence of the ESR line shift $\delta B = B_{res} - B_0$ measured in $Cu_{1-x}Ni_xGeO_3$ at two given temperatures. (b) Evolution with the nickel concentration of the relative line shift measured at two different temperatures in four $Cu_{1-x}Ni_xGeO_3$ single crystals. These two figures establish the proportionality (a) between the line shift and the frequency at given temperature and Ni concentration, and (b) between the relative shift and the Ni concentration, at a given temperature (see the solid lines).

$T/T_{SP}=1$ with the curve of the pure sample. One can note the good agreement between this curve and the I'_{ESR} data. This analysis further supports the idea that the ESR signal only comes from the Cu^{2+} spins. We will come back to these results when discussing the line shift results (see Sec. V B). The same study has been performed for a magnetic field applied along the *a* axis, and the results were found to be similar.

2. Linewidth

Besides the large ESR shift, the other main qualitative effect of Ni doping is a very large broadening of the ESR line as compared to pure $CuGeO_3$. This is further contrasted by the linewidth data of $CuGeO_3$ doped by the nonmagnetic impurities Zn, Mg, or Si.[27] In Fig. 7(a), the low-temperature linewidth data are presented at the *X* band for pure $CuGeO_3$ and various Ni-doping levels. It appears that above T_{SP} and up to about 40 K, the linewidth increases linearly with temperature, and is approximately proportional to the Ni concentration at a rate of $\Delta B/x \sim 1000$ G/%Ni for $T=20$ K and a slope $\Delta B/(x.T) \sim 100$ G.K^{-1}/%Ni.

However, as shown in Fig. 7(b), contrary to the pure $CuGeO_3$ linewidth data, where the linear temperature dependence extends almost up to room temperature (see also Refs. 19 and 20), the Ni-doped $CuGeO_3$ ESR linewidth reaches a plateau above 50 K independent of both the temperature and the magnetic field. This plateau is proportional to the Ni concentration at a rate $\Delta B_{plateau}/x \simeq 4600$ G/%Ni. At temperatures lower than T_{SP}, a temperature behavior much closer to that of pure $CuGeO_3$ is observed, with a comparable rate of broadening [see Fig. 7(a)], but now strongly increasing with field [see Fig. 7(b)]. Whereas at present we cannot account for the temperature dependence of the linewidth, the order of magnitude of $\Delta B_{plateau}$ is discussed in Sec. V B.

3. Line shift along the c axis

We now focus on the ESR line shift $\delta B = B_{res} - B_0$, measured for $B\|c$, B_{res} being the resonance field of the studied sample and B_0 the resonance field of pure $CuGeO_3$ (corresponding to $g_c=2.05$) measured at the same frequency. The aim of the following analysis is to study the field (or frequency), concentration and temperature dependence of the shift in order to derive an expression of $\delta B(f,x,T)$ experimentally.

Figure 8(a) shows the frequency dependence of the line shift measured for two different samples, 0.85 and 2% Ni-doped $CuGeO_3$, and two different temperatures. This figure shows that the shift is proportional to the working frequency (see solid lines) and thus to B_0, which proves that it is a genuine "*g* shift." This shift increases with *x* and T^{-1}. To study the concentration and temperature dependences, we will thus now refer to the frequency-independant relative shift $\delta B/B_0$. Figure 8(b) shows the Ni concentration dependence of $\delta B/B_0$ at two given temperatures $T=20$ and 50 K (data from various frequencies were combined to obtain this figure). For both temperatures, the relative shift is proportional to the Ni concentration, up to 3% (see the solid lines).

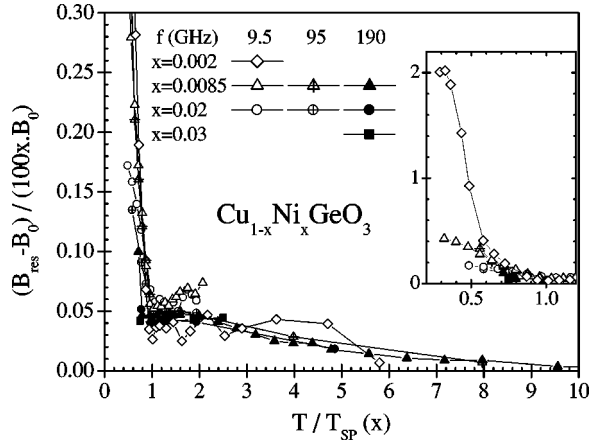

FIG. 9. Relative line shift $\delta B/B_0$ normalized by the Ni concentration (divided by $100x$) as a function of the reduced temperature $T/T_{SP}(x)$ for all studied Ni-doped $CuGeO_3$ samples (various concentrations at various frequencies). The inset shows the low-temperature part.

At this stage, we thus have the relation

$$\frac{\delta B}{B_0}(x,T) = C(T)x. \tag{3}$$

All our experimental results for the line shift are gathered in Fig. 9 using the above relation, i.e., the relative line shift normalized to the Ni concentration $\delta B/(100xB_0)$ is plotted as a function of the reduced temperature $T/T_{SP}(x)$. This figure shows the good agreement of relation (3) with our data. All the experimental points are roughly on a unique curve $C(T)$, at least above T_{SP}. Below the spin-Peierls temperature, the temperature dependence of $\delta B/B_0$ depends on the Ni-doping level. Indeed, the data at 9.5 and 95 GHz are well superimposed down to $0.7T_{SP}$ for both samples with $x = 0.0085$ and 0.02, but the increase at lower temperature is stronger as the Ni concentration decreases (see the inset of Fig. 9).

Thus, in order to study in detail the temperature dependence of the shift, we separately consider the paramagnetic (P) and SP phases. The temperature dependence of the relative shift in the 0.85% Ni-doped sample is illustrated for two different frequencies in Figs. 10(a) for $T > T_{SP}$ and 11(a) for $T < T_{SP}$. Between 300 and 20 K, $\delta B/B_0$ increases up to 4% [see Fig. 10(a)] and its temperature dependence behaves like the nickel susceptibility $\chi_{Ni}(T)$ [see Fig. 10(b)]. The latter was derived by subtracting the susceptibility of pure $CuGeO_3$ to that of the Ni-doped sample [both presented in Fig. 1(b)]. The inset of Fig. 10(b) shows that $\delta B(T)/B_0$ is strictly proportional to $\chi_{Ni}(T)$ in the P phase.

Concerning the low-temperature part, one can note a strong enhancement of the line shift below 12.5 K at 9.5 and 190 GHz [see Fig. 11(a)]. This temperature corresponds to the SP transition; thus this behavior is mainly related to the dimerization of the Cu ions into $S=0$ states. Figure 11(b) illustrates the temperature dependence of the inverse of the Cu-dimer susceptibility (the spin-Peierls contribution in the triplet state $S=1$) $\chi_{Cu}(T)$, which was obtained by subtracting a Curie-Weiss contribution (coming from the Ni ions) to the total susceptibility.[13] As can be seen in the inset of Fig. 11(b), $\delta B(T)/B_0(T)$ varies linearly with $1/\chi_{Cu}(T)$. This analysis of the data leads to the following relation for the relative shift:

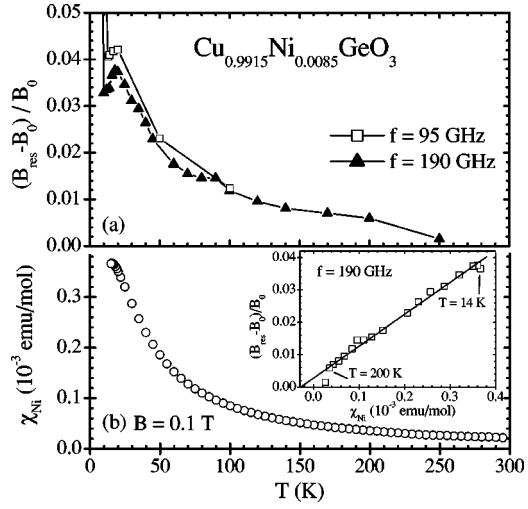

FIG. 10. Temperature dependence in the paramagnetic phase of (a) the relative ESR line shift and (b) the static susceptibility of the Ni ions, measured in $Cu_{0.9915}Ni_{0.0085}GeO_3$. The inset of (b) illustrates the relative ESR line shift as a function of the Ni susceptibility, at each temperature.

$$\frac{\delta B}{B_0}(x,T) \propto x \frac{\chi_{Ni}(T)}{\chi_{Cu}(T)}. \tag{4}$$

For the same reason as for the integrated intensities (the decrease of the fraction K_{SP} when x increases), this formula is indeed consistent with the inset of Fig. 9, where the rela-

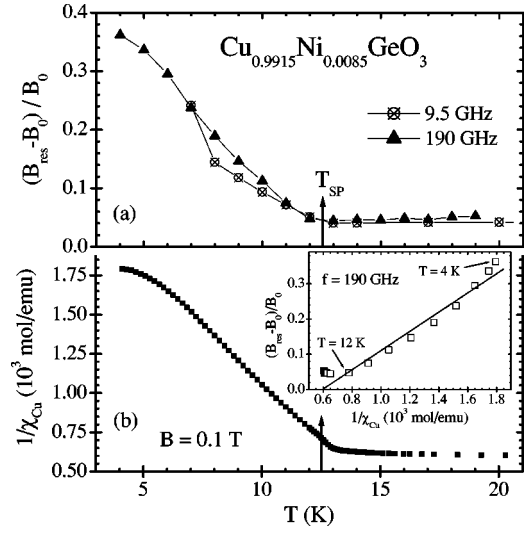

FIG. 11. Temperature dependence in the spin-Peierls phase of (a) the relative ESR line shift and (b) the inverse static susceptibility of the Cu dimers, measured in $Cu_{0.9915}Ni_{0.0085}GeO_3$. The inset of (b) illustrates the relative ESR line shift as a function of the inverse Cu susceptibility, at each temperature.

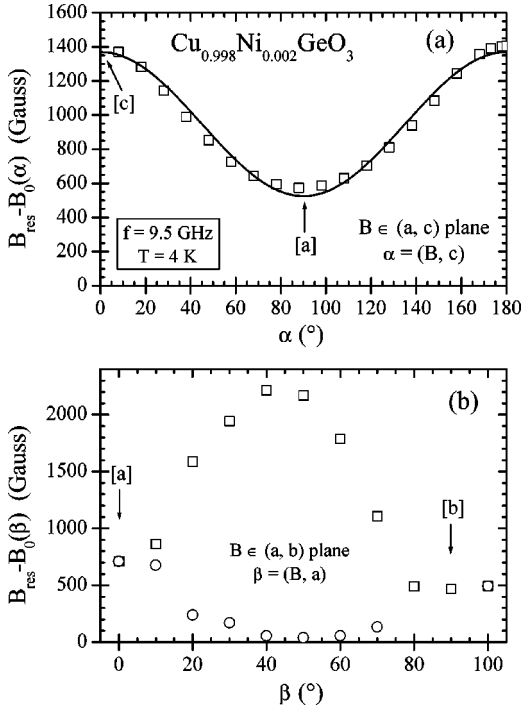

FIG. 12. Anisotropy of the ESR line shift in the (a,c) and (a,b) planes measured in the X band, at $T=4$ K in 0.2% Ni-doped $CuGeO_3$. The open squares correspond to the aforementioned ESR line and the open circles to the additional line that appears in the (a,b) plane.

tive shift below T_{SP} shows a fourfold increase as the Ni doping level decreases from 0.85% to 0.2%.

4. Anisotropy of the line shift

The anisotropy of the line shift has also been carefully studied at the X band in the 0.2% Ni-doped compound at 4 K, in the (a,c) and (a,b) planes (see Fig. 12). The shift δB was found to be very anisotropic in both planes, and a second, less intense, resonance line was observed in the (a,b) plane.

In the (a,c) plane, the shift is maximum along c ($\simeq$1400 G), and minimum along b ($\simeq$600 G), following $\delta B(\alpha)=\delta B_{ac}+\delta B_{anis}\cos\alpha$ with $\delta B_{ac}\simeq 950$ and $\delta B_{anis}\simeq 420$ G. In the (a,b) plane, the shift is minimum and equivalent along the a and b axes while a maximum shift (2200 G) is found at $\beta\simeq 45°$ (where β is the angle between the applied magnetic field and the a axis), possibly reflecting the anisotropy of the Cu to the Ni site coupling. Note that the anisotropy of the line shift along the crystal axes follows that of the static susceptibility [see Fig. 2(b) for the 6% Ni-doped $CuGeO_3$ sample].

B. Resonance model

The model used to interpret the ESR data of $CuGeO_3$ doped with Ni at very low concentrations is constrained by the above-mentioned experimental observations, which we briefly recall.

(i) At all temperatures along the a, b, and c directions, only one Lorentzian-shaped (except at the lowest temperature) ESR line is observed, above and below the spin-Peierls transition, which we attribute to the paramagnetic Cu^{2+} spins above T_{SP} and to the excited triplet Cu^{2+} spins below T_{SP}.

(ii) No resonance consistent with Ni^{2+} in a distorted octahedral site is observed in the temperature range $4<T<300$ K, neither at 9.5 GHz nor up to 190 GHz and 10 T.

(iii) The ESR-integrated intensity, normalized to the resonance field, does not scale with the static susceptibility measured in the same Ni-doped sample, but only to the proportion of Cu spins being in the SP triplet state, which supports (i).

(iv) The width of the Cu^{2+} resonance strongly increases with the Ni concentration (at a rate of 0.1 T/% Ni at 20 K).

(v) A resonance shift of the Cu^{2+} line toward higher fields, proportional to the concentration of the Ni^{2+} ions, is observed above and below the spin-Peierls transition. This shift is proportional to the Ni ion susceptibility, and inversely proportional to the Cu ion susceptibility. This shift thus becomes particularly noticeable below the SP transition. The shift is anisotropic, being roughly twice as large for the c direction as for the a and b directions, which are about equivalent: it then appears that this shift is not related to the g-factor anisotropy of the pure $CuGeO_3$ system ($g_a=2.15$, $g_b=2.26$, and $g_c=2.05$).

A very detailed investigation of a two-coupled-paramagnetic-spin system, present in $RbMnF_3$ doped with Ni, Co or Fe, was performed by Gulley and Jaccarino.[31] For 1–5 % Ni doping, contrary to the present work, no discernible linewidth broadenings together with a small g shift of 0.5% are observed. This situation was quantitatively analyzed in terms of very strongly exchange-coupled Ni and Mn spins. This is clearly not the case for $CuGeO_3$:Ni, but does apply to the case of $CuGeO_3$:Zn, :Mg, or :Si. Indeed, in addition to the absence of broadening and to the 1% g shift, the fact that the ESR-integrated intensity fits well the static susceptibility constitutes compelling evidence of strong coupling between the bulk Cu^{2+} spins and the Cu^{2+} spins induced by the nonmagnetic impurities.

The model used for our interpretation is an extension of Kittel's analysis for the ferrimagnetic resonance shift in the presence of strongly relaxing rare-earth dopants.[32] Indeed, the coupling $J_c\simeq 120$–180 K of the Cu^{2+} spins along each of the two (nonequivalent[22]) one-dimensional chains of $CuGeO_3$ is strong enough to ensure that a single, exchange-narrowed mode prevails in the presence of an antiferromagnetic coupling J_N induced by a Ni^{2+} $S=1$ spin on its two Cu^{2+} near neighbors. In order to account for our observation of a single resonance line, we are forced to assume that (i) either the relaxation rate of the Ni^{2+} spin is sufficiently large, compared to J_N, to decouple the Ni^{2+} spins from the precession of the Cu^{2+} spins; or that (ii) this decoupling occurs through a sufficiently large zero-field splitting removing the Ni^{2+} resonance away from the Cu^{2+} resonance. In this case, we can model the spin dynamics of $CuGeO_3$:Ni by two coupled Bloch-like equations: one for the tightly coupled together Cu^{2+} spin system (magnetization $\vec{M}$), and one for the fast relaxing Ni^{2+} spins (magnetization $\vec{N}$). For

the sake of simplicity we will assume that the gyromagnetic ratio $\gamma_{Cu} \simeq \gamma_{Ni} = \gamma$, so that the decoupling occurs only through the relaxation rate of the Ni^{2+} spins. The coupled equations are then written with T_{Ml}^{-1} the Cu spin-lattice relaxation rate, T_{Nl}^{-1} the Ni spin-lattice relaxation rate, and T_{MN} and T_{NM} the Cu/Ni spin-spin cross relaxation rates between Cu and Ni (related by $T_{MN}/T_{NM} = N^0/M^0$, i.e., the ratio of the equilibrium magnetizations, by detailed balance[33]):

$$\frac{d\vec{M}}{dt} = \gamma \vec{M} \times (\vec{H} + \lambda \vec{N}) - \frac{\vec{M}}{T_{MN}} + \frac{\vec{N}}{T_{NM}} - \frac{\vec{M} - \vec{M}^0}{T_{Ml}}, \quad (5)$$

$$\frac{d\vec{N}}{dt} = \gamma \vec{N} \times (\vec{H} + \lambda \vec{M}) - \frac{\vec{N}}{T_{NM}} + \frac{\vec{M}}{T_{MN}} - \frac{\vec{N} - \vec{N}^0}{T_{Nl}}. \quad (6)$$

Solving for the transverse components as usual leads to the determinant

$$\begin{vmatrix} \Omega_N & \lambda_N \\ \lambda_M & \Omega_M \end{vmatrix} = 0 \quad (7)$$

with

$$\Omega_M = \omega - \omega_0 - iT_{Ml}^{-1} - \lambda_M, \quad (8)$$

$$\Omega_N = \omega - \omega_0 - iT_{Nl}^{-1} - \lambda_N, \quad (9)$$

$$\lambda_M = \gamma \lambda M^0 + iT_{NM}^{-1}, \quad (10)$$

$$\lambda_N = \gamma \lambda N^0 + iT_{MN}^{-1}, \quad (11)$$

where ω_0 is the unshifted resonance frequency. In the limit of $T_{Nl}^{-1} \to \infty$, we obtain[34]

$$\omega - \omega_0 = \lambda \gamma N^0 + i(T_{MN}^{-1} + T_{Ml}^{-1}). \quad (12)$$

This yields indeed a Cu^{2+} resonance shifted to higher fields if $\lambda < 0$, i.e., an antiferromagnetic coupling from Ni^{2+} to Cu^{2+}, and proportional to the Ni^{2+} static magnetization N^0. However, a major difference appears between our $CuGeO_3$:Ni model and Kittel's two-sublattice model. In classical sublattice spin dynamics the coupling constant λ represents the exchange energy density through $-\lambda \vec{M}_A . \vec{M}_B$, meaning that every spin A is coupled to every spin B. In our case, we want to specify that the Ni spin is coupled to its two first nearest neighbors Cu^{2+} by J_N, and that the effective coupling λ is the resulting average of the Cu-Ni exchange J_N among the Cu^{2+} spins (tightly coupled through J_c). This average coupling λ occurs, however, only from those Cu^{2+} spins which are not condensed into singlets $S=0$ below the spin-Peierls transition. Writing that the exchange energy density is identical in both descriptions yields

$$\lambda = \frac{2J_N}{\hbar^2 \gamma^2} \frac{1}{(1 - n_{SP})\mathcal{N}}, \quad (13)$$

where n_{SP} is the fraction of condensed singlet spins, i.e., the spin-Peierls order parameter and $\mathcal{N}$ is the number of Cu ions per unit volume. The shift is then given by

$$\omega - \omega_0 = \frac{2J_N}{\hbar^2 \gamma} \frac{N^0}{(1 - n_{SP})\mathcal{N}}. \quad (14)$$

Thus Eq. (14) indeed predicts the observed dependence for the line shift [see Eq. (4)]. The merit of this formulation is that we use the same argument above and below T_{SP}. The above equation can be rewritten (in the P phase) in terms of our measured quantities to yield J_N by

$$J_N = \frac{1}{2}(g\mu_B)^2 N_A \left[\frac{\delta B / B_0}{\chi_{Ni}^0} \right]. \quad (15)$$

The term between square brackets is depicted in the inset of Fig. 10(b). We find $J_N = 75 \pm 10$ K where the error is estimated from the spread of the data at various x and frequencies. This value for J_N was checked to be quite consistent with the weak coupling approximation. However, this value is three times larger than the one obtained above (Sec. IV) from the fit to the static susceptibility. We think that the value of J_N derived from the ESR data is closer to the truth, since the zero-field splitting of the Ni^{2+} ion was not incorporated into the susceptibility analysis: This parameter is *a priori* not required in the ESR model, since Ni^{2+} is considered ''nonresonant.''

As concerns the linewidth, a direct application of the weak-coupling exchange broadening calculated by Gulley and Jaccarino [Eq. (2.12) of Ref. 31], with $J = J_c \simeq 150$ K and $J' = J_N \simeq 75$ K, yields a temperature-independent broadening of 8000 G/% Ni, to be compared with 4600 G/% Ni observed between 50 and 300 K.

VI. ANTIFERROMAGNETIC RESONANCE IN Ni-DOPED $CuGeO_3$

Typical AFMR signals measured in the $x = 0.04$ sample at 1.8 K in a field applied along the *a*, *b*, and *c* axes are shown in Fig. 13. Five ESR lines were observed at 21.87 GHz for $B \| a$. The lines at 0.3, 1.2, and 1.5 T correspond to AFMR lines. The line at 0.75 T originates from a standard DPPH (1,1-diphenyl-2-picrylhydrazyl) sample. The line at 0.7 T probably corresponds to an electron paramagnetic resonance (EPR) signal from the sample. For $B \| b$ and $B \| c$, one ESR line, which corresponds to an AFMR signal, was observed around 47.5 GHz. The EPR signal which was observed along the *a* axis in the AF-ordered state was not observed for these two field directions.[35] This is consistent with a recent theory[36] which predicted the existence of an EPR signal even in the ordered phase when the external field is applied parallel to the easy axis.

From the AFMR results, we can identify the easy, second-easy, and hard axes as the *a*, *c*, and *b* axes, respectively, as will be shown below. The angular dependence of the resonance fields at the *X* band was also measured. Resonance points around 0.9 T show a minimum when the field is parallel to the *a* axis. From this result we confirmed that the spins point along the *a* axis within an experimental error of $\sim 2°$, which was not clearly determined by the susceptibility[18] and neutron-scattering measurements.[7] We

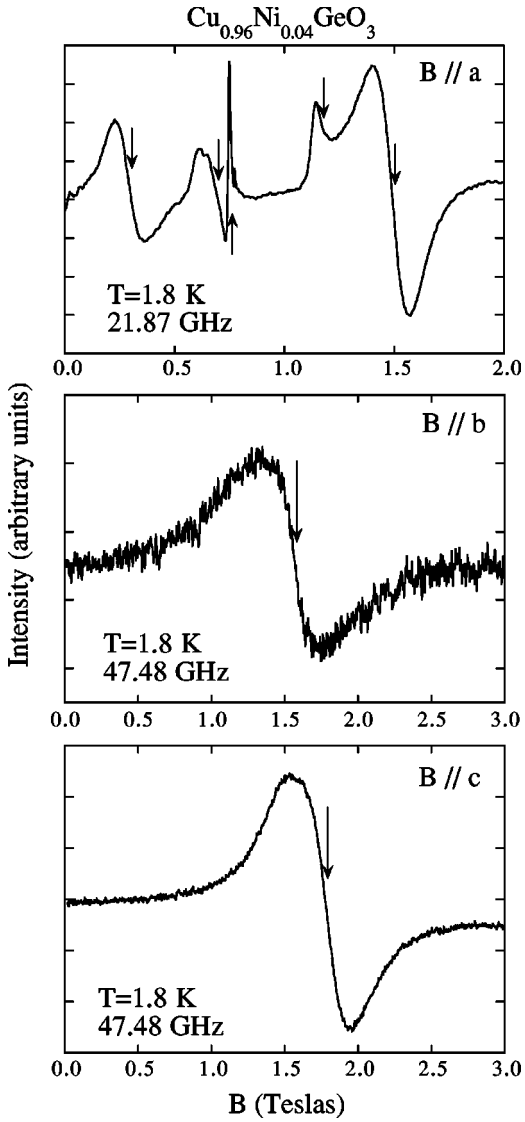

FIG. 13. Typical ESR signals in a single crystal of $Cu_{0.96}Ni_{0.04}GeO_3$ at 1.8 K for the three crystallographic orientations.

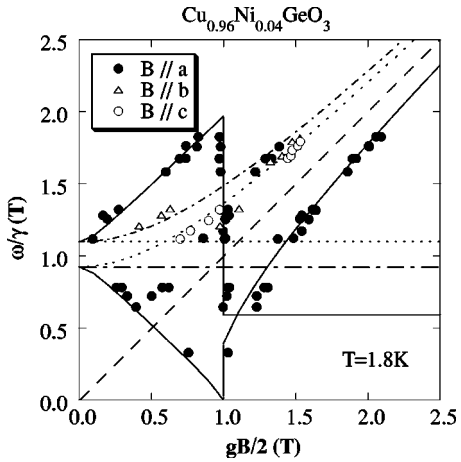

FIG. 14. The frequency vs magnetic-field diagram of the resonance points at 1.8 K in a $Cu_{0.96}Ni_{0.04}GeO_3$ single crystal. Closed circles, open triangles, and open circles denote experimental data, and solid, dash-dotted, and dotted curves are theoretical ones for $B\|a$, b, and c, respectively.

also performed an AFMR measurement in the $x=0.03$ sample at $T=1.8$ K. The AFMR signals are less clear mainly due to the lower T_N. However, it was found that the magnetic anisotropy is the same as in the $x=0.04$ sample.

Figure 14 shows the frequency vs magnetic-field plot of the resonance points at 1.8 K. Here the angular frequency (ω) is divided by $\gamma \equiv 2\pi g \mu_B / h$ (μ_B is the Bohr magneton, h is Planck's constant) to express it in magnetic-field units, and B is scaled by the g value for the respective field directions. The g values we used are $g_a=1.72$, $g_b=1.80$, and $g_c=1.65$, which are 80% of the g values in pure $CuGeO_3$, and are also consistent with those obtained from ESR measurements at ~ 5 K. The data were analyzed with the AFMR theory for a two-sublattice antiferromagnet with orthorhombic anisotropy.[37] This theory was used in analyzing Zn- (Refs. 15 and 16) and Si-doped samples,[17] and was conveniently reviewed in Ref. 38. We obtained the parameters $C_1(=2AK_1)=0.85$ (T^2), $C_2(=2AK_2)=1.2$ (T^2), and α $(=1-\chi_\parallel/\chi_\perp)=0.90$, where A, K_i ($i=1$ and 2), $\chi_\parallel$, and $\chi_\perp$ are the molecular field coefficient, the anisotropy constants, and the susceptibilities along the easy axis and perpendicular to it, respectively. The lines in Fig. 14 are fits with the classical AFMR theory. The parameter α obtained with AFMR measurements is similar to those in $Cu_{0.96}Zn_{0.04}GeO_3$ (Refs. 15 and 16) and $CuGe_{0.98}Si_{0.02}O_3$,[17] as shown in Table II, but is much larger than that obtained from the magnetic susceptibility measurements ($\alpha \sim 0.35$). The susceptibility parallel to the a axis of $Cu_{0.96}Ni_{0.04}GeO_3$ does not go to zero with decreasing temperature below T_N, as shown in Fig. 2(a). This is quite different from what a classical theory of antiferromagnetism predicts for $\chi_\parallel$. We found that the measured χ_a can be interpreted as a sum of a paramagnetic susceptibility which obeys the Curie law and an antiferromagnetic one. The amount of the paramagnetic ''centers'' is estimated to be about 1% of the total spins assuming $S=\frac{1}{2}$ and $g=2.1$. The antiferromagnetic susceptibility decreases with decreasing temperature more rapidly than χ_a, thus giving a larger value for α.

We now discuss the origin of the magnetic anisotropy in Ni-doped $CuGeO_3$. In order to explain this, we consider three terms; single ion anisotropy (E_{SI}), dipole-dipole (E_D), and anisotropic exchange (E_{AE}) energies. Moriya and Yosida theoretically discussed the origin of the anisotropy in $CuCl_2 \cdot 2H_2O$.[39] They considered both E_D and E_{AE} terms

TABLE II. Observed C_1, C_2, and α in $CuGeO_3$ doped with Si, Zn, and Ni.

Impurity	T_N (K)	C_1 (T^2)	C_2 (T^2)	α
Si (2%)[a]	4.8	1.3 ± 0.1	3.8 ± 0.2	0.78 ± 0.06
Zn (4%)[b]	4.2	0.89	2.1	0.85
Ni (4%)	4.0	0.85	1.2	0.90

[a]Reference 17.
[b]Reference 15.

(note that no E_{SI} term is possible for Cu^{2+} spin). They estimated $|E_D| \sim 10^{-4}$ cm^{-1}/ion and $|E_{AE}| \sim 10^{-3}$ cm^{-1}/ion, respectively. Although the crystal structure of $CuGeO_3$ is different from that of $CuCl_2 \cdot 2H_2O$, we expect that the value of E_D in $CuGeO_3$ is not very much different from the one given above. For E_{AE} in $CuGeO_3$, we estimate a value ten times larger, because the exchange interaction is about ten times larger than for $CuCl_2 \cdot 2H_2O$. On the other hand, $|E_{SI}| \sim 1$ cm^{-1}/ion for Ni^{2+} (Ref. 40) so that even a small amount of doping will change the anisotropy of the system drastically. The g value and the single-ion anisotropy constant D, for Ni^{2+} in an axially distorted octahedral environment, are related to the spin-orbit coupling and to the crystal-field levels. In the well-documented case of trigonal elongation of the octahedron, as in $CsNiF_3$,[41] this distortion leads to $D>0$ [and $g_\perp(\mathrm{Ni}) > g_\parallel(\mathrm{Ni})$]. In contrast, in the case of $CuGeO_3$, one expects the axial elongation to yield $D<0$ similar to the Tutton salts,[42] and hence to give rise to an easy local axis perpendicular to c. Here we denote the single-ion anisotropy term as DS_z^2.

The easy axis for Ni^{2+} spin in $CuGeO_3$ lies in the ab plane, and is directed alternately when one moves from one site to the other along the b axis. Because of the antiferromagnetic interaction, the spins will point either close to the a or b axis, with an antiferromagnetic arrangement along the b axis, the former being favored by E_D. Thus the mean easy axis is the a axis. Then the easy and second easy axes in Zn- and Si-doped samples are interchanged in the Ni-doped sample.

The C_1 and C_2 values for various impurity-doped $CuGeO_3$ are summarized in Table II. C_1 and C_2 correspond to the geometric mean of the exchange field and anisotropy fields along the second-easy and hard axes, respectively. It is noted that the two parameters are very close in the Ni-doped sample. The parameter C_2 is related to the anisotropy when one rotates the magnetic moments from the c to b axes in $CuGeO_3$:Zn, and from the a to b axes in $CuGeO_3$:Ni. In the Zn-doped sample, one loses both E_D and E_{AE} for this rotation, while in the Ni-doped sample E_D and a part of E_{AE} are lost (E_{AE} in the ab plane is less anisotropic because g_a and g_b are nearly equal). So C_2 in the Ni-doped sample is smaller than that in the Zn-doped sample. Consequently, C_1 and C_2 become closer in the $CuGeO_3$:Ni sample.

VII. CONCLUSION

In this paper we have presented a systematic study of the spin-resonance properties of $CuGeO_3$ in the paramagnetic, spin-Peierls, and antiferromagnetic regimes, when doped with Ni, and compared these results with previously obtained ESR data on $CuGeO_3$ doped with nonmagnetic impurities such as Zn, Mg or Si. The main conclusions that we are able to draw are the following.

(1) Whereas the investigation of the static susceptibility of doped $CuGeO_3$ enables us to define a universal behavior, in the proper reduced units, for the appearance of the paramagnetic, spin-Peierls and antiferromagnetic phases in the temperature-concentration diagram, at least two different regimes exist as concern the ESR properties, depending on whether the doping atom is magnetic or not.

(2) In the case of nonmagnetic doping, the resulting Cu^{2+} moments responsible for the Curie tail observed below the spin-Peierls temperature T_{SP} are in a strong-coupling regime with a spin-Peierls excited triplet, resulting in an unshifted ESR line and a c-direction easy axis in the AFMR analysis.

(3) In the presence of doping with $S=1$ Ni^{2+}, a weak coupling is found from the analysis of the measured large shift of the Cu^{2+} ESR, both in the paramagnetic and spin-Peierls regimes.

(4) However, in order to account for the AFMR a-easy axis in the latter case, one has to assume that the Ni^{2+} ions do participate in the AFMR mode. The origin of the anisotropy in this case is the single-ion anisotropy of Ni^{2+} rather than the anisotropic exchange present for pure and (nonmagnetic) doped $CuGeO_3$.

(5) Although each of these different regimes can be consistently parametrized in a quantitative way, a general description of the dynamics of the transverse spin susceptibilities of doped spin-Peierls compounds is still an open question.

ACKNOWLEDGMENTS

We thank A. K. Hassan for helpful discussions and for the high-field EPR of $CuGeO_3$:Zn single crystals. This work was partially supported by the ''MR Science Research Program'' from RIKEN. We would like to thank M. Tokunaga for his help in the AFMR measurement. The Institut d'Electronique Fondamentale and Laboratoire de Physico-Chimie de l'Etat Solide are Unités Mixtes de Recherche CNRS: UMR 8622 and UMR 8648, respectively.

*Present address: Advanced Science Research Center, Japan Atomic Energy Research Institute, Tokai, Ibaraki 319-1195, Japan
†Also at RIKEN Harima Institute, Mikazuki, Sayo, Hyogo 679-5148, Japan

[1] M. Hase, I. Terasaki, and K. Uchinokura, Phys. Rev. Lett. **70**, 3651 (1993).
[2] J.-P. Pouget, L.-P. Regnault, M. Ain, B. Hennion, J.-P. Renard, P. Veillet, G. Dhalenne, and A. Revcolevschi, Phys. Rev. Lett. **72**, 4037 (1994).
[3] M. Hase, I. Terasaki, Y. Sasago, K. Uchinokura, and H. Obara, Phys. Rev. Lett. **71**, 4059 (1993).
[4] M. Hase, Y. Sasago, K. Uchinokura, G. Kido, and T. Hamamoto, J. Magn. Magn. Mater. **140-144**, 1691 (1995).
[5] S.B. Oseroff, S.-W. Cheong, B. Aktas, M.F. Hundley, Z. Fisk, and L.W. Rupp, Jr., Phys. Rev. Lett. **74**, 1450 (1995).
[6] J.G. Lussier, S. Coad, D.F. McMorrow, and D. McK Paul, J. Phys.: Condens. Matter **7**, L325 (1995).
[7] S. Coad, J.-G. Lussier, D.F. McMorrow, and D. McK Paul, J. Phys.: Condens. Matter **8**, 6251 (1996).
[8] T. Masuda, A. Fujioka, Y. Uchiyama, I. Tsukada, and K. Uchinokura, Phys. Rev. Lett. **80**, 4566 (1998).
[9] J.-P. Renard, K. Le Dang, P. Veillet, G. Dhalenne, A. Revcolevschi, and L.-P. Regnault, Europhys. Lett. **30**, 475 (1995).

[10] L.-P. Regnault, J.-P. Renard, G. Dhalenne, and A. Revcolevschi, Europhys. Lett. **32**, 579 (1995).
[11] Y. Sasago, N. Koide, K. Uchinokura, M.C. Martin, M. Hase, K. Hirota, and G. Shirane, Phys. Rev. B **54**, R6835 (1996).
[12] H. Fukuyama, T. Tanimoto, and M. Saito, J. Phys. Soc. Jpn. **65**, 1182 (1996).
[13] B. Grenier, J.-P. Renard, P. Veillet, C. Paulsen, G. Dhalenne, and A. Revcolevschi, Phys. Rev. B **58**, 8202 (1998).
[14] M. Hase, K. Uchinokura, R.J. Birgeneau, K. Hirota, and G. Shirane, J. Phys. Soc. Jpn. **65**, 1392 (1996).
[15] M. Hase, M. Hagiwara, and K. Katsumata, Phys. Rev. B **54**, R3722 (1996).
[16] P. Fronzes, M. Poirier, A. Revcolevschi, and G. Dhalenne, Phys. Rev. B **56**, 7827 (1997).
[17] H. Nojiri, T. Hamamoto, Z.J. Wang, S. Mitsudo, M. Motokawa, S. Kimura, H. Ohta, A. Ogiwara, O. Fujita, and J. Akimitsu, J. Phys.: Condens. Matter **9**, 1331 (1997).
[18] N. Koide, Y. Sasago, T. Masuda, and K. Uchinokura, Czech. J. Phys. **46**, 1981 (1996).
[19] S. Oseroff, S-W. Cheong, A. Fondado, B. Aktas, and Z. Fisk, J. Appl. Phys. **75**, 6819 (1994).
[20] I. Yamada, M. Nishi, and J. Akimitsu, J. Phys.: Condens. Matter **8**, 2625 (1996).
[21] M. Honda, T. Shibata, K. Kindo, S. Sugai, T. Takeuchi, and H. Hori, J. Phys. Soc. Jpn. **65**, 691 (1996).
[22] B. Pilawa, J. Phys.: Condens. Matter **9**, 3779 (1997).
[23] M. Hase, J. Magn. Magn. Mater. **177-181**, 611 (1998).
[24] A.K. Hassan, L.A. Pardi, G.B. Martins, G. Cao, and L.-C. Brunel, Phys. Rev. Lett. **80**, 1984 (1998).
[25] V.N. Glazkov, A.I. Smirnov, O.A. Petrenko, D.M.K. Paul., A.G. Vetkin, and R.M. Eremina, J. Phys.: Condens. Matter **10**, 7879 (1998).
[26] B. Grenier, J.-P. Renard, P. Veillet, C. Paulsen, R. Calemczuk, G. Dhalenne, and A. Revcolevschi, Phys. Rev. B **57**, 3444 (1998).
[27] Among the 12 investigated samples (doped with 1.6, 3.9, and 10% Zn, 1, 3, and 5% Mg, 0.2, 0.7, 0.85, 1.5, 6, and 8.5% Si), the linewidth was found to be always the same as in pure $CuGeO_3$ except for the 0.7% Si- and 3.9% Zn-doped samples, where a temperature-independent constant broadening (of $\simeq 200$ G along *a* and *c*, and $\simeq 400$ G along *b*) was measured.
[28] M. Hase, N. Koide, K. Manabe, Y. Sasago, K. Uchinokura, and A. Sawa, Physica B **215**, 164 (1995).
[29] B. Grenier and P. Monod (unpublished).
[30] Note that the results from the 0.2% Ni-doped sample and the pure one can be directly compared on the same *T* scale, since the spin-Peierls temperatures are very close to each other (see Table I).
[31] J.E. Gulley and V. Jaccarino, Phys. Rev. B **6**, 58 (1972).
[32] C. Kittel, Phys. Rev. **115**, 1587 (1959).
[33] S.E. Barnes, Adv. Phys. **30**, 801 (1981).
[34] In Kittel's paper, due to the particular form of the damping specific to ferrimagnetic materials, a special case of strong coupling in the presence of infinite relaxation rate is obtained. This results in a shift which is independent from the coupling contrary to Eq. (12) of the present work. The latter is simply related to the ''unbottleneck'' situation.
[35] This fact shows that this EPR line cannot be attributed to free Cu spins [see, for instance, M. Hagiwara, K. Katsumata, I. Yamada, and H. Suzuki, J. Phys.: Condens. Matter **8**, 7349 (1996)]. However, we note that the 0.5 T linewidth of the 3.2% Ni sample used by Glazkov *et al.* (Ref. 25, Fig. 3) precludes a detailed comparison with the present results obtained on high-quality samples (0.2 T linewidth).
[36] A. Ogasahara and S. Miyashita, J. Phys. Soc. Jpn. **69**, 4043 (2000).
[37] T. Nagamiya, K. Yosida, and R. Kubo, Adv. Phys. **4**, 1 (1955).
[38] K. Katsumata, J. Phys.: Condens. Matter **12**, R589 (2000).
[39] T. Moriya and K. Yosida, Prog. Theor. Phys. **9**, 663 (1953).
[40] A. Abragam and B. Bleaney, *Electron Paramagnetic resonance of transition ions* (Clarendon Press, Oxford, 1970), p. 450.
[41] See, for instance, C. Dupas and J.-P. Renard, J. Phys. C **10**, 5057 (1977).
[42] J.H.E. Griffiths and J. Owen, Proc. R. Soc. London, Ser. A **213**, 459 (1952).